The Open Civil Engineering Journal
DOI: 10.2174/0118741495497082260924115750, 2026, 20, e18741495497082
ISSN: 1874-1495

RESEARCH ARTICLE OPEN ACCESS

Pore Structure and Microstructural Characteristics of Cement Paste Incorporating Cuttlebone Powder

Chakkarphan Sangsuwan[1], Worachai Ponloa[2,*], Pim Hathaipichitchai[3], Sonthaya Khamdech[2], Somboon Asawarujanon[2] and Pitpatpol Thanyamaneelertsakul[2]

[1]*Faculty of Engineering, Rajamangala University of Technology Phra Nakhon, Bangkok, Thailand*
[2]*Faculty of Engineering, Bangkokthonburi University, Bangkok, Thailand*
[3]*Faculty of Agricultural Technology and Industrial Technology, Nakhon Sawan Rajabhat University, Nakhon Sawan, Thailand*

Abstract:

Introduction/Objective: Cement manufacturing generates high CO_2 emissions, requiring clinker replacement materials that maintain hydration-controlled structural development. Marine bio-calcium provides an aragonite-based calcium source. This study evaluates the effects of Cuttlebone Powder (CBP) on pore structure and microstructural characteristics under increasing CBP replacement levels.

Methods: The study prepared ordinary Portland cement pastes containing 10–50% CBP at a water-to-binder ratio of 0.50 and cured the specimens for 28 days. Mercury Intrusion Porosimetry (MIP), Scanning Electron Microscopy (SEM), and SEM–EDS measured pore parameters and elemental composition.

Results: Porosity decreased from 30.72% in the control paste to 21.72% at 40% CBP. Average pore diameter decreased from 0.0713 µm to 0.0217–0.0249 µm in the 20–40% CBP range. Cumulative intrusion volume decreased from 0.2239 mL/g in the control paste to 0.1377–0.1633 mL/g within the 20–40% CBP range. Ca atomic percentage increased from 66.45% to 82.50%, while Si decreased from 30.87% to 15.73%. Ca/Si increased from 2.15 in the control paste to 2.6–3.5 in PPC20–PPC40 and reached 5.25 at 50% CBP.

Discussion: Pore refinement and a denser matrix are observed in CBP-modified cement paste. The 20–40% replacement range provides the most pronounced changes in pore structure and microstructural characteristics under the tested conditions.

Conclusion: CBP modifies pore structure and Ca/Si in cement paste. The 20–40% replacement range provides the strongest pore refinement under the tested conditions. These results indicate the potential of CBP as a bio-calcium additive for cement systems.

Keywords: Cuttlebone powder, Cement paste, Pore structure, Bio-calcium, Microstructure, Hydration product, Calcium carbonate.

© 2026 The Author(s). Published by Bentham Open.
This is an open access article distributed under the terms of the Creative Commons Attribution 4.0 International Public License (CC-BY 4.0), a copy of which is available at: https://creativecommons.org/licenses/by/4.0/legalcode. This license permits unrestricted use, distribution, and reproduction in any medium, provided the original author and source are credited.

*Address correspondence to this author at the Department of Civil Engineering, Faculty of Engineering, Bangkok Thonburi University, Bangkok, Thailand; E-mail: worachai.pon@bkkthon.ac.th

Cite as: Sangsuwan C, Ponloa W, Hathaipichitchai P, Khamdech S, Asawarujanon S, Thanyamaneelertsakul P. Pore Structure and Microstructural Characteristics of Cement Paste Incorporating Cuttlebone Powder. Open Civ Eng J, 2026; 20: e18741495497082. http://dx.doi.org/10.2174/0118741495497082260924115750

Received: April 18, 2026
Revised: July 08, 2026
Accepted: July 17, 2026
Published: October 01, 2026

Send Orders for Reprints to
reprints@benthamscience.net

1. INTRODUCTION

The cement industry faces increasing sustainability pressure because cement manufacturing remains a major contributor to global greenhouse gas emissions. Recent reviews report that cement production contributes approximately 7% of global anthropogenic CO_2 emissions, highlighting the urgency of emission reduction strategies [1]. Cement manufacturing also releases CO_2 during limestone calcination and consumes high thermal energy during kiln operation, and these processes intensify environmental impacts [2, 3]. Consequently, engineers increasingly adopt blended cement systems and partial clinker replacement using supplementary cementitious materials to reduce clinker content [4]. This strategy promotes waste utilization and circular economy principles because industrial by-products and recycled materials substitute clinker and improve resource efficiency while reducing environmental impacts and landfill burden [4, 5]. However, replacement strategies must maintain cement functionality and long-term performance because hydration reactions control strength development and durability in cementitious systems [3]. Alternative materials therefore influence hydration reactions and microstructural evolution, and these changes directly control engineering performance under low-carbon design approaches [6]. Researchers must therefore understand how replacement materials interact with hydration processes, and this requirement motivates further investigation of specific alternative materials in subsequent sections.

Calcium carbonate additions are receiving increasing attention in cementitious systems because they reduce clinker consumption and maintain hydration and engineering performance [7, 8]. Limestone powder is the most established carbonate material and primarily acts as a mineral filler that improves particle packing and promotes early hydration through physical dispersion within blended cement matrices [8, 9]. Fine carbonate particles provide additional nucleation sites for hydration products and can promote early cement hydration [10]. Calcium carbonate precipitation within available pore spaces contributes to pore filling and changes the pore structure of cementitious matrices [8, 11]. Carbonate phases also interact chemically with aluminate components to form carboaluminate hydrates, and this reaction modifies phase assemblage and supports microstructural development during hydration [9, 10]. Calcite- and aragonite-dominated materials exhibit different nucleation efficiencies and hydration responses, and these differences directly influence hydration behavior [10, 12]. Consequently, bio-derived carbonate resources obtained from biological or waste streams attract growing attention, and these materials provide sustainability benefits and distinct physicochemical characteristics, and these properties warrant further investigation in cementitious systems [7].

Bio-derived calcium carbonate has emerged as an alternative material for partial cement replacement, supporting sustainable cement systems and promoting marine waste valorization [13-15]. Marine biogenic wastes, particularly seashell residues from seafood processing industries, provide abundant calcium and support resource recovery strategies aligned with low-carbon construction practices [13, 16]. These biomaterials originate from biological mineralization processes and exhibit hierarchical porous morphologies that increase surface complexity and promote interaction with cement hydration environments compared with conventional limestone [14, 17]. Cuttlebone predominantly consists of aragonite-type calcium carbonate, which distinguishes it from conventional calcite-based carbonate materials [18]. Seashell-derived calcium carbonate can provide nucleation sites for hydration products and promote microstructural development in blended cement systems [14]. However, the behavior of seashell-derived materials in cementitious systems remains insufficiently understood, and researchers still face uncertainties regarding interactions with hydration processes, phase evolution, and pore–microstructure consequences [16, 17]. Therefore, focused studies are needed to clarify the role of marine skeletal bio-calcium materials in cement hydration and evaluate their suitability for engineering cement systems.

Cuttlebone Powder (CBP) is a marine-derived bio-calcium material obtained from seafood processing waste [18, 19]. Cuttlebone consists mainly of aragonite-type calcium carbonate ($CaCO_3$) [19, 20]. Conventional limestone fillers predominantly contain calcite [19]. X-Ray Diffraction (XRD) and Fourier-Transform Infrared Spectroscopy (FTIR) analyses confirmed the aragonite-rich composition of cuttlebone [19]. Cuttlebone also exhibits a highly porous, hierarchical architecture composed of lamellar chambers separated by interconnected walls [20]. The mineralogical composition and porous architecture of CBP differ from those of conventional carbonate materials and make CBP a potential calcium-rich material for sustainable applications [18-20].

Researchers have used CBP in engineering applications as a sustainable calcium-rich material [21, 22]. CBP originates from cuttlefish bone and consists mainly of aragonite-type $CaCO_3$, unlike conventional limestone-based materials, which are predominantly composed of calcite [19-21]. Previous studies used CBP as a partial cement replacement in green concrete and demonstrated its feasibility as an alternative calcium carbonate source in cementitious systems [21]. Aragonite and calcite exhibit different crystal morphologies, stabilities, dissolution behaviors, and interactions with cement hydration processes [21, 23, 24]. Calcium carbonate polymorphs also influence hydration kinetics, microstructural development, and mechanical performance through their morphology and nucleation behavior [12, 23, 24]. These characteristics distinguish CBP from conventional calcium carbonate materials and support its use as an aragonite-rich bio-calcium resource in cementitious systems. Although previous studies have reported several applications of CBP, further attention should be given to its effects on pore structure development and microstructural characteristics of cement paste.

This study investigates cement paste incorporating cuttlebone powder as a marine bio-calcium modifier. The work evaluates pore structure characteristics, microstructural features, and localized elemental compositions under increasing CBP replacement levels. MIP, SEM, and SEM–EDS analyses were used to examine changes in pore structure, matrix morphology, and Ca/Si ratios within the investigated cement paste system.

2. MATERIALS AND METHODS

2.1. Materials

Ordinary Portland Cement (OPC) was used as the primary binder. The OPC was manufactured by Siam City Cement Public Company Limited, Thailand, under the commercial designation Diamond. The cement conformed to ASTM C150 [25]. The CBP was produced from the cuttlebone of *Sepia aculeata* originating from the Gulf of Thailand and was used as a partial cement replacement. The cuttlebone was cleaned, dried, and mechanically ground into a fine powder before use. The powder passed through a No. 100 sieve (150 µm) to produce a uniform particle size before mixing with cement.

The CBP consisted mainly of aragonite-structured calcium carbonate and served as a bio-derived calcium source within the cement matrix. The preparation used deionized water for all paste mixtures, and the mixtures contained no chemical admixtures. This approach isolated the influence of CBP on pore structure and microstructural development.

2.2. Mix Proportion and Sample Preparation

CBP was used as a partial replacement for OPC at replacement levels of 0, 10, 20, 30, 40, and 50% by mass. A constant water-to-cement ratio of 0.50 was maintained for all mixtures. The mixture proportions are presented in Table **1**.

2.3. Specimen Preparation

All specimens were prepared by mixing cement paste according to ASTM C305 [26] using a mechanical mixer. After mixing, the fresh paste was cast into molds with dimensions of 50 mm × 50 mm × 50 mm following ASTM C109 [27], and left for 24 h. The specimens were then demolded and cured in water according to ASTM C511 [28] at a controlled temperature of 23 ± 2 °C for 28 days. After curing, the specimens were immersed in an acetone solution to stop the hydration reaction. The specimens were cut into prism-shaped pieces with dimensions of approximately 5 mm × 5 mm × 25 mm for MIP testing. The remaining portions were prepared for SEM observation and SEM–EDS analysis.

2.4. Mercury Intrusion Porosimetry (MIP)

The pore structure of cement paste was measured by Mercury Intrusion Porosimetry (MIP). After acetone treatment, the prism-shaped specimens were air-dried under laboratory conditions at 25 ± 2 °C for 24 h before testing. The test provided pore size distribution, cumulative intrusion volume, total accessible porosity, and threshold pore diameter. These parameters were used to evaluate pore refinement and pore structure characteristics of the cement paste mixtures.

2.5. Scanning Electron Microscopy (SEM)

The experiment examined microstructural characteristics using Scanning Electron Microscopy (SEM). The specimens were prepared to preserve the internal morphology of the cement paste before observation. The SEM analysis focused on hydration products, gel formation, and matrix densification. The obtained images were used to evaluate microstructural changes associated with increasing CBP replacement levels.

2.6. Energy Dispersive Spectroscopy (SEM-EDS)

The experiment performed elemental analysis using SEM-EDS. Elemental compositions were obtained from SEM-EDS area analysis of selected microstructural regions. The measurement quantified relative calcium and silicon contents within the analyzed areas. The analysis calculated Ca/Si trends to support interpretation of chemical variation among mixtures.

3. RESULTS

3.1. Pore Structure from Mercury Intrusion Porosimetry

The dominant peak of the control specimen is located at approximately 0.07–0.09 µm, with a noticeable contribution from pores larger than 0.1 µm, as shown in Fig. (**1**). Increasing the CBP replacement level from PPC10 to PPC30 shifts the peak toward smaller pore diameters. PPC20–PPC40 exhibit peak positions near 0.02–0.03 µm. PPC50 exhibits a broader pore size distribution and a wider pore diameter range than PPC10–PPC40. No further reduction in the dominant pore diameter is observed beyond PPC40.

Table 1. Mixture proportions of the specimens.

S. ID.	W/b ratio	OPC (wt.%)	CBP (wt.%)
Control	0.5	100	0
PPC10	0.5	90	10
PPC20	0.5	80	20
PPC30	0.5	70	30
PPC40	0.5	60	40
PPC50	0.5	50	50

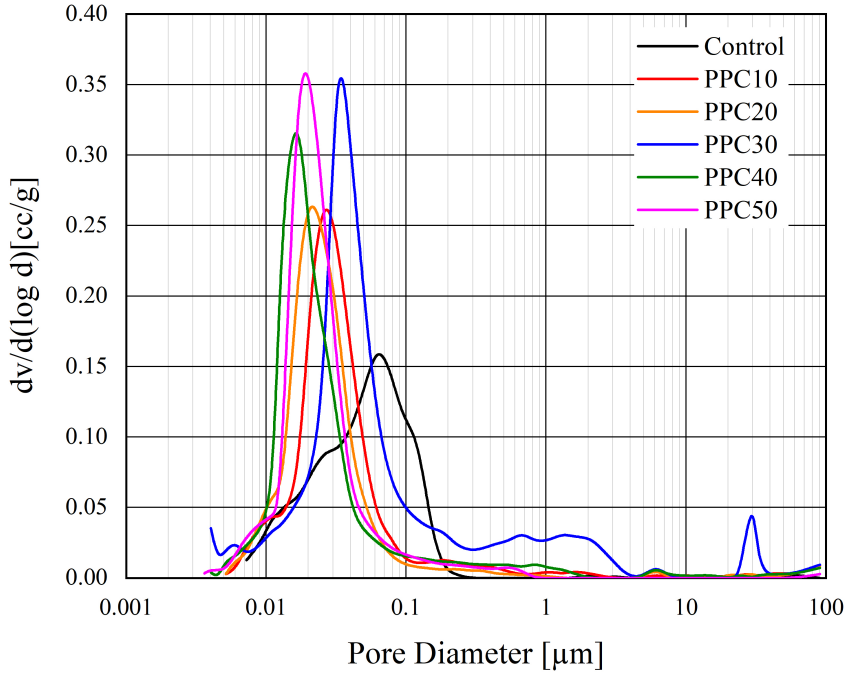

Fig. (1). Pore size distribution of cement paste mixtures obtained from mercury intrusion porosimetry.

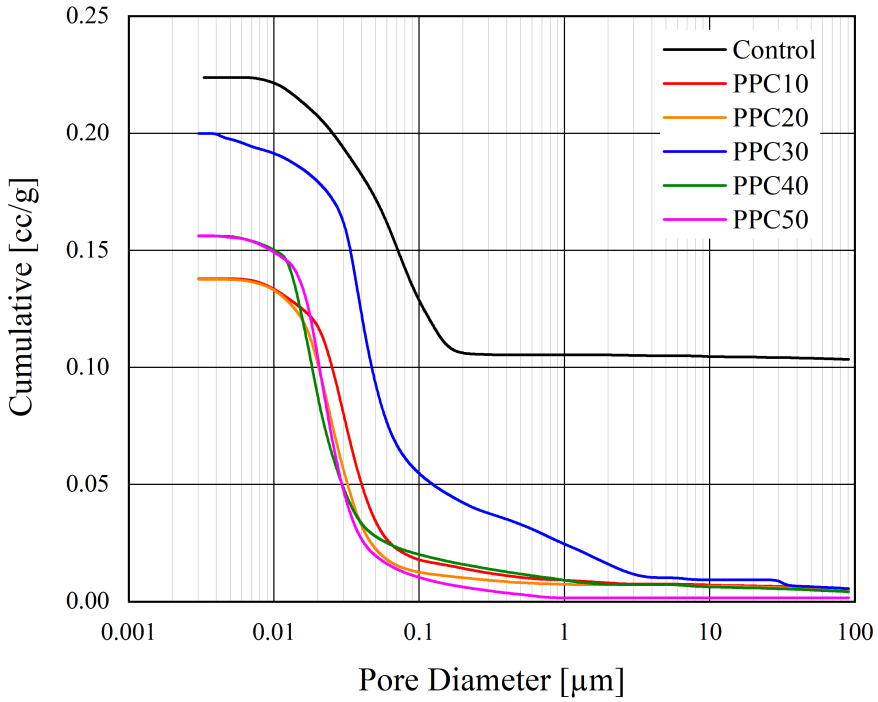

Fig. (2). Cumulative pore volume of cement paste mixtures obtained from mercury intrusion porosimetry.

Lower cumulative intrusion volumes are observed in the CBP blended mixtures. Figure 2 shows that the control specimen records the highest value of 0.2239 mL/g. PPC20, PPC30, PPC40, and PPC50 exhibit values of 0.1562, 0.1633, 0.1377, and 0.1379 mL/g, respectively. The lowest cumulative intrusion volumes occur in PPC40 and PPC50. Further increasing the CBP replacement level from 40% to 50% does not produce additional reduction.

Porosity decreases from 30.72% in the control specimen to 21.72% in PPC40, a reduction of approximately 29%, as summarized in Table 2. The cumulative intrusion volume decreases from 0.2239 to 0.1377 mL/g. The average pore diameter decreases from 0.0713 µm in the control specimen to 0.0217–0.0249 µm in PPC20–PPC40. PPC20–PPC40 exhibit lower porosity and smaller average pore diameters than the control specimen, whereas PPC50 does not show additional reduction. The control specimen records the highest cumulative intrusion volume of 0.2239 mL/g, porosity of 30.72%, and average pore diameter of 0.0713 µm among all mixtures. These results indicate a greater volume of accessible pores in the control specimen than in the CBP-blended mixtures. PPC20–PPC50 exhibit cumulative intrusion volumes of 0.1377–0.1633 mL/g, porosity values of 21.72–24.35%, and average pore diameters of 0.0217–0.0298 µm. Increasing CBP beyond 40% does not produce further measurable improvement in pore structure parameters.

3.2. SEM Microstructural Observation

SEM observations in Fig. (3a–f) confirm the structural transition observed in the MIP results. The control paste in Fig. (3a) shows a discontinuous hydration network with visible capillary pathways. Increasing CBP content in Fig. (3b–e) promotes matrix continuity and reduces visible pore domains. The transition becomes most evident in PPC20–PPC40. In this range, Ca/Si increases from 2.61 to 3.47, and pore diameter decreases by approximately 65–70% compared with pure OPC. These coupled geometric and compositional changes indicate internal reorganization of hydration products rather than simple pore filling.

Table 2. Summary of MIP pore structure parameters.

S. ID.	Total Intrusion Volume (mL/g)	Total Pore Area (m^2/g)	Average Pore Diameter (µm)	Porosity (%)	Threshold Pressure (psi)
Control	0.2239	12.549	0.0713	30.72	5.73
PPC10	0.1999	21.695	0.0369	29.15	5.04
PPC20	0.1562	28.785	0.0217	23.77	5.92
PPC30	0.1633	28.175	0.0222	24.35	5.04
PPC40	0.1377	22.150	0.0249	21.72	5.29
PPC50	0.1379	18.500	0.0298	21.90	2.78

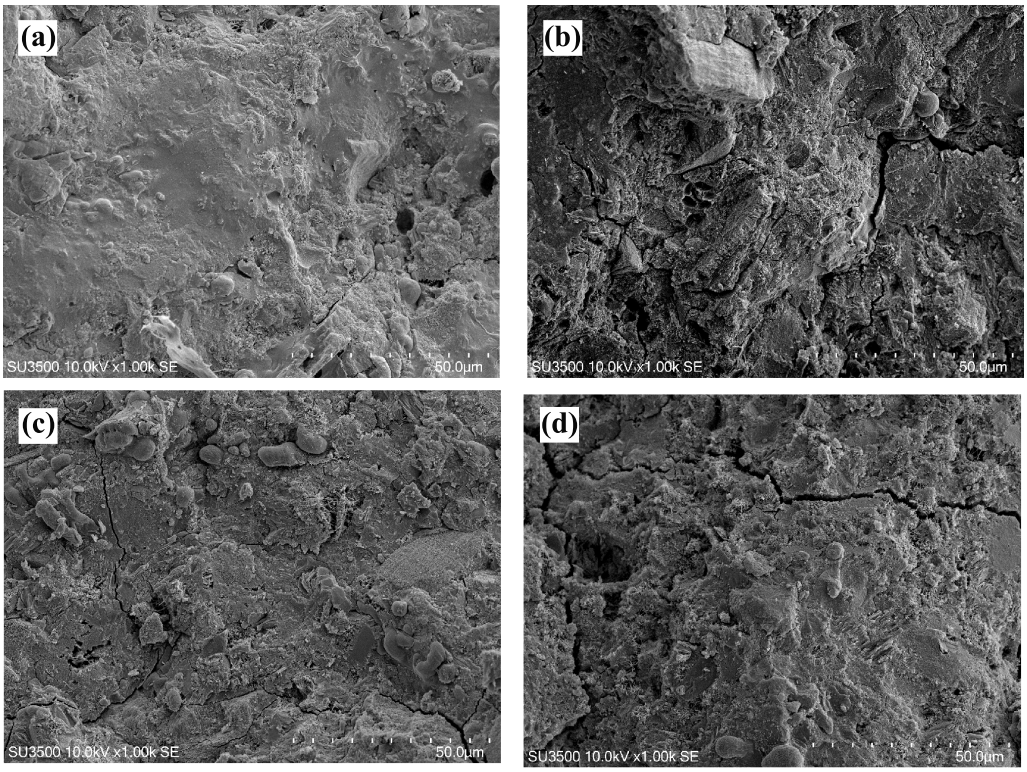

Fig. 3 contd.....

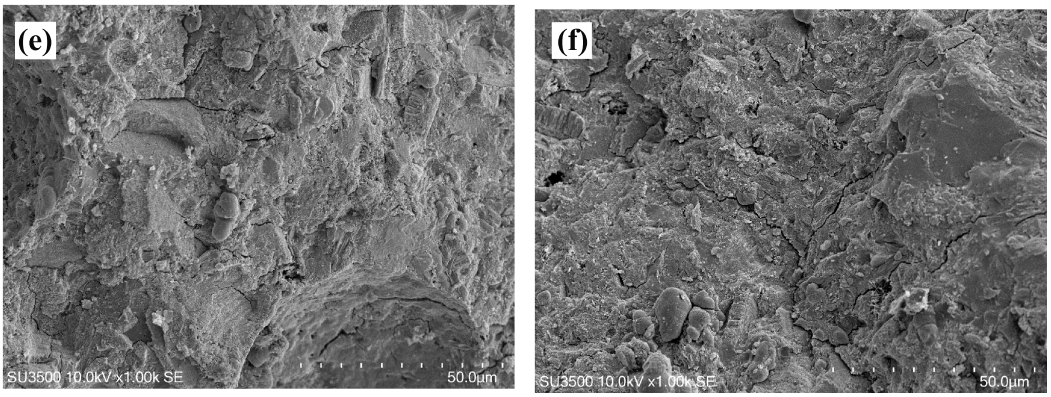

Fig. (3). SEM micrographs of cement paste at 28 days showing progressive hydration, packing continuity, and reduction of visible pore pathways with increasing CBP replacement: (**a**) Control, (**b**) PPC10, (**c**) PPC20, (**d**) PPC30, (**e**) PPC40, and (**f**) PPC50.

At 50% CBP replacement, the microstructure in Fig. (**3f**) remains dense. However, additional refinement does not occur. The absence of further morphological change indicates structural saturation at high CBP content. The SEM evidence supports the MIP results and shows that bio-calcium CBP modifies hydration packing and pore connectivity through a coupled structural–compositional effect.

3.3. SEM-EDS

The reported elemental compositions were obtained from SEM–EDS area analysis of selected regions. The control paste in Fig. (**4a**) shows 66.45% Ca and 30.87% Si, which gives a Ca/Si ratio of 2.15. This value falls within the upper range typically reported for hydrated Portland cement systems (≈1.5–2.2). Increasing CBP replacement in Fig. (**4b–f**) raises Ca content and reduces Si content, as also summarized in Fig. (**5**) . The Ca/Si ratio therefore increases continuously and reaches 5.25 at 50% replacement. PPC20–PPC40 in Fig. (**4c–e**) show Ca/Si values between 2.6 and 3.5, and this range coincides with the lowest porosity and smallest average pore diameter measured by MIP. PPC50 in Fig. (**4f**) increases the Ca/Si ratio further, but only minor changes are observed in the pore parameters.

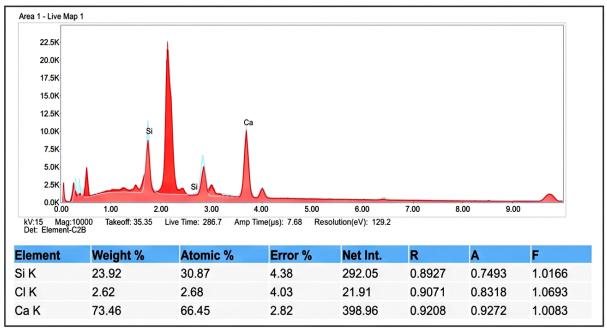

Element	Weight %	Atomic %	Error %	Net Int.	R	A	F
Si K	23.92	30.87	4.38	292.05	0.8927	0.7493	1.0166
Cl K	2.62	2.68	4.03	21.91	0.9071	0.8318	1.0693
Ca K	73.46	66.45	2.82	398.96	0.9208	0.9272	1.0083

(a) Control

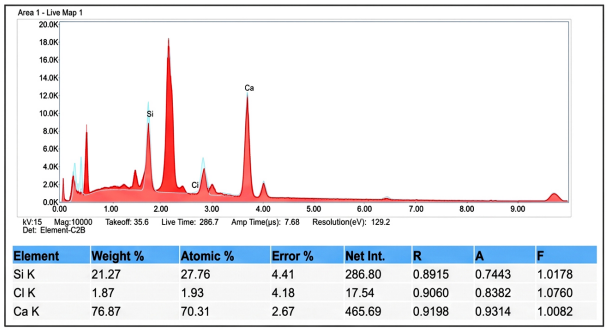

Element	Weight %	Atomic %	Error %	Net Int.	R	A	F
Si K	21.27	27.76	4.41	286.80	0.8915	0.7443	1.0178
Cl K	1.87	1.93	4.18	17.54	0.9060	0.8382	1.0760
Ca K	76.87	70.31	2.67	465.69	0.9198	0.9314	1.0082

(b) PPC10

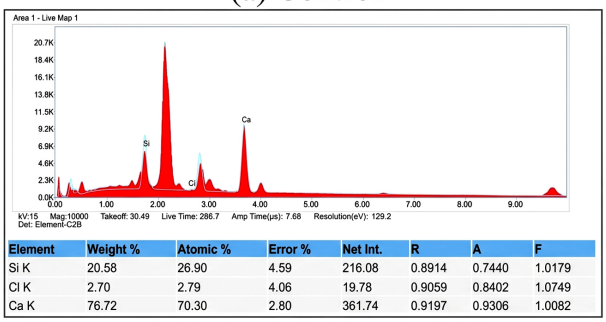

Element	Weight %	Atomic %	Error %	Net Int.	R	A	F
Si K	20.58	26.90	4.59	216.08	0.8914	0.7440	1.0179
Cl K	2.70	2.79	4.06	19.78	0.9059	0.8402	1.0749
Ca K	76.72	70.30	2.80	361.74	0.9197	0.9306	1.0082

(c) PPC20

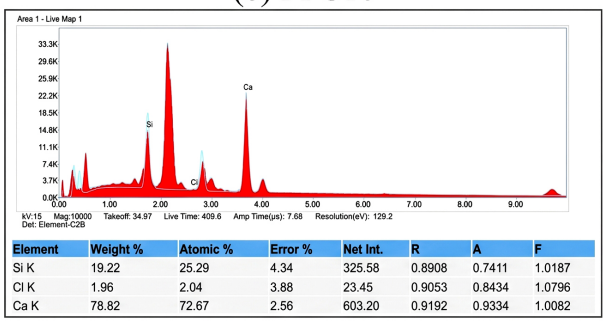

Element	Weight %	Atomic %	Error %	Net Int.	R	A	F
Si K	19.22	25.29	4.34	325.58	0.8908	0.7411	1.0187
Cl K	1.96	2.04	3.88	23.45	0.9053	0.8434	1.0796
Ca K	78.82	72.67	2.56	603.20	0.9192	0.9334	1.0082

(d) PPC30

Fig. 4 contd.....

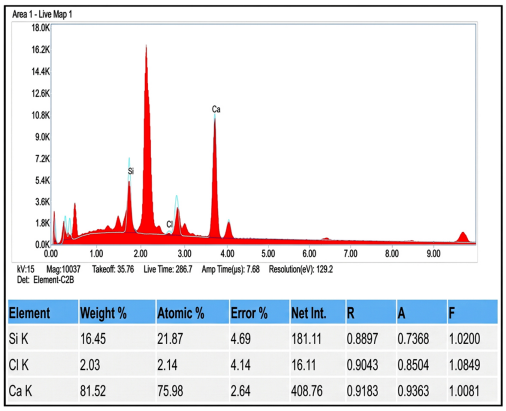

Element	Weight %	Atomic %	Error %	Net Int.	R	A	F
Si K	16.45	21.87	4.69	181.11	0.8897	0.7368	1.0200
Cl K	2.03	2.14	4.14	16.11	0.9043	0.8504	1.0849
Ca K	81.52	75.98	2.64	408.76	0.9183	0.9363	1.0081

(e) PPC40

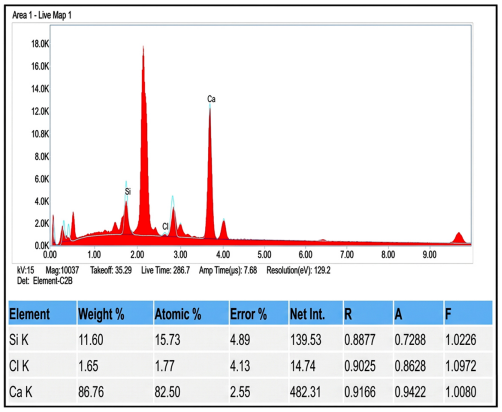

Element	Weight %	Atomic %	Error %	Net Int.	R	A	F
Si K	11.60	15.73	4.89	139.53	0.8877	0.7288	1.0226
Cl K	1.65	1.77	4.13	14.74	0.9025	0.8628	1.0972
Ca K	86.76	82.50	2.55	482.31	0.9166	0.9422	1.0080

(f) PPC50

Fig. (4). Representative SEM-EDS spectra of cement pastes: (**a**) Control, (**b**) PPC10, (**c**) PPC20, (**d**) PPC30, (**e**) PPC40, and (**f**) PPC50.

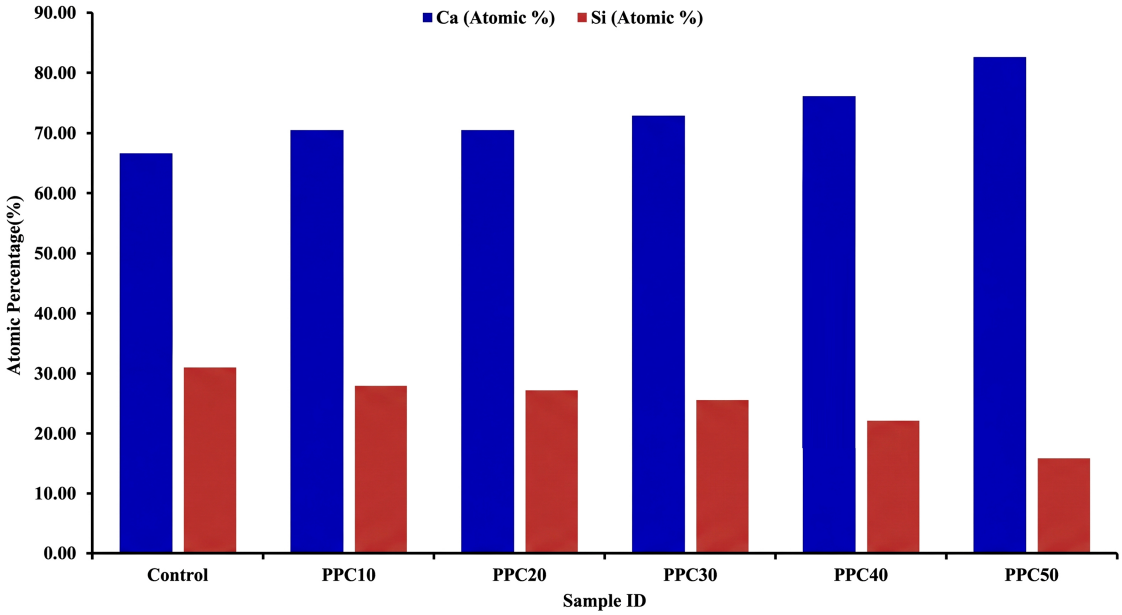

Fig. (5). Variation of Ca and Si atomic percentage in cement paste samples incorporating CBP determined by SEM–EDS analysis.

Si, Cl, and Ca elemental maps for Control, PPC20, PPC40, and PPC50 are included in Fig. (**6**) . The mapping results follow the same compositional trends as the SEM–EDS area analysis. These results show that the Ca/Si ratio increases with CBP replacement. PPC20–PPC40 exhibit lower porosity and smaller average pore diameters than the control paste, whereas PPC50 shows only minor additional changes in these parameters.

4. DISCUSSION

The MIP results show changes in pore structure after CBP replacement. The control paste exhibits dominant medium capillary pores near 0.07–0.09 µm, whereas PPC20–PPC40 exhibit dominant pore diameters near 0.02–0.03 µm. Porosity decreases from 30.72% to 21.72%, and cumulative intrusion volume decreases accordingly. SEM images show fewer observable voids and a denser matrix in the CBP mixtures than in the control paste. These observations are consistent with the lower porosity and cumulative intrusion volumes measured by MIP. The shift toward smaller pore diameters indicates that CBP replacement modifies the pore structure by reducing the proportion of larger capillary pores.

SEM observations show a less compact microstructure with visible pore pathways in the control paste. In contrast, the CBP mixtures exhibit fewer observable voids and a denser matrix. These observations agree with the lower porosity and cumulative intrusion volumes measured by MIP. The SEM observations therefore support the pore refinement identified by MIP.

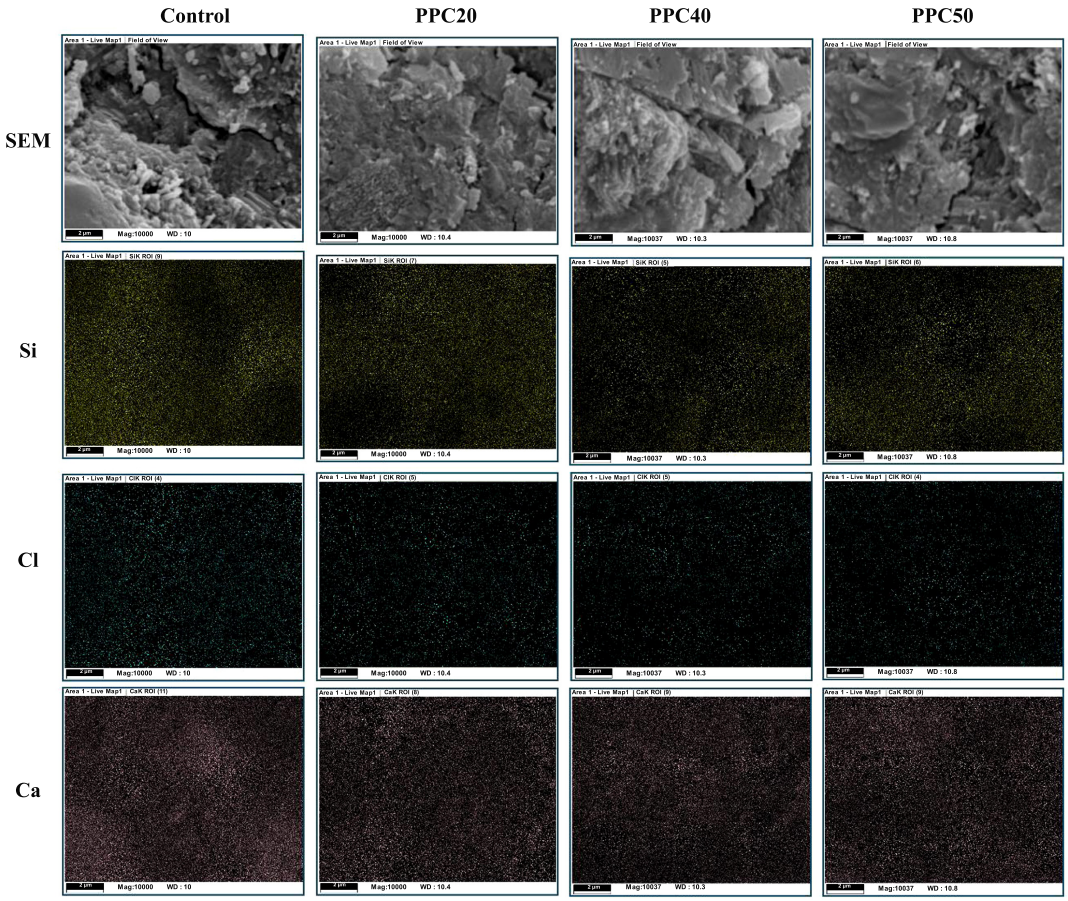

Fig. (6). SEM micrographs and corresponding EDS elemental maps of Si, Cl, and Ca for Control, PPC20, PPC40, and PPC50.

The Ca/Si ratio increases from 2.15 in the control paste to 2.6–3.5 in PPC20–PPC40. This compositional range coincides with the lowest porosity and smallest pore diameters measured by MIP. Higher Ca/Si ratios indicate increased calcium content within the analyzed regions. The measured values represent localized elemental compositions obtained from EDS analysis rather than individual phase compositions. The EDS and MIP results show similar trends in PPC20–PPC40.

Further increasing CBP replacement to 50% raises the Ca/Si ratio to 5.25; however, SEM images and pore structure parameters show limited additional refinement. PPC50 exhibits porosity, cumulative intrusion volume, and average pore diameter values comparable to those of PPC40. In contrast, larger changes in these parameters are observed between the control paste and PPC20–PPC40. Most pore structure refinement occurs within the CBP replacement range of 20–40%, whereas increasing the replacement level from 40% to 50% produces only minor additional changes.

PPC20–PPC40 exhibit lower porosity, smaller pore diameters, lower cumulative intrusion volumes, and a denser matrix than the control paste. In contrast, increasing the CBP replacement level to 50% produces only minor additional changes in pore structure and morphology. The Ca/Si ratio, pore structure parameters, and SEM observations show similar trends across the mixtures.

5. LIMITATIONS OF THE STUDY

This study evaluated the pore structure and microstructure of CBP-modified cement paste using MIP, SEM, and EDS at 28 days. The MIP analysis used one specimen from each mixture without replication. Therefore, the quantitative pore parameters represent the tested specimens and should not be interpreted as statistically representative values. MIP characterizes accessible pore structure but does not directly identify the hydration mechanisms responsible for pore refinement. SEM–EDS provides localized information from selected areas and does not represent the complete distribution of hydration products within the cement matrix. The study also used a single water-to-binder ratio and curing condition. Longer curing ages are needed to examine changes in pore structure and microstructure over time. Different mixture conditions should also be considered. XRD analysis is needed to identify hydration products and phase changes associated with CBP incorporation. This information can support the interpretation of pore structure development in CBP-modified cement paste.

CONCLUSION

CBP replacement modifies the pore structure, microstructure, and elemental composition of cement paste. MIP results show a shift from medium capillary pores toward smaller pore domains, accompanied by reductions in porosity, cumulative intrusion volume, and average pore diameter. SEM observations show fewer observable voids and a denser matrix in the CBP mixtures than in the control paste. SEM–EDS area analysis indicates increasing Ca/Si ratios with increasing CBP replacement. The most pronounced pore structure refinement occurs within the CBP replacement range of 20–40%, which exhibits lower porosity, smaller pore diameters, and lower cumulative intrusion volumes. Further increasing the replacement level to 50% increases the Ca/Si ratio but produces only minor additional changes in the measured pore structure parameters. The results demonstrate a relationship between pore structure, matrix morphology, and localized elemental composition within the investigated cement paste system.

AUTHORS' CONTRIBUTIONS

The authors confirm their contributions to the paper as follows: C.S.: Study conception and design; W.P.: Designed the experimental plan, prepared the materials, and conducted the laboratory experiments; P.H., S.K., S.A., and P.T.: Conceptualized and designed the experimental program, analyzed and interpreted the data, and drafted the manuscript, contributed to laboratory experiments, data analysis, and interpretation. All authors approved the final version of the manuscript.

LIST OF ABBREVIATIONS

CBP	=	Cuttlebone Powder
EDS	=	Energy Dispersive Spectroscopy
FTIR	=	Fourier Transform Infrared Spectroscopy
MIP	=	Mercury Intrusion Porosimetry
OPC	=	Ordinary Portland Cement
SEM	=	Scanning Electron Microscopy
w/b	=	Water-to-Binder Ratio
XRD	=	X-Ray Diffraction

CONSENT FOR PUBLICATION

Not applicable.

AVAILABILITY OF DATA AND MATERIALS

The data supporting the findings of this study are available from the corresponding author, [W.P], upon reasonable request.

FUNDING

None.

CONFLICT OF INTEREST

The authors declare no conflict of interest, financial or otherwise.

ACKNOWLEDGEMENTS

The authors acknowledge Rajamangala University of Technology Phra Nakhon, Bangkok, Thailand, for laboratory facilities and technical support.

REFERENCES

[1] R. Supriya, R. Chaudhury, U. Sharma, P.C. Thapliyal, and L.P. Singh, "Low-CO2 emission strategies to achieve net zero target in cement sector", *J. Clean. Prod.,* vol. 417, p. 137466, 2023. [http://dx.doi.org/10.1016/j.jclepro.2023.137466]

[2] E. Benhelal, E. Shamsaei, and M.I. Rashid, "Challenges against CO2 abatement strategies in cement industry: A review", *J. Environ. Sci.,* vol. 104, pp. 84-101, 2021. [http://dx.doi.org/10.1016/j.jes.2020.11.020] [PMID: 33985750]

[3] S. Barbhuiya, F. Kanavaris, B.B. Das, and M. Idrees, "Decarbonising cement and concrete production: Strategies, challenges and pathways for sustainable development", *J. Build. Eng.,* vol. 86, p. 108861, 2024. [http://dx.doi.org/10.1016/j.jobe.2024.108861]

[4] H. Dahanni, A. Ventura, L. Le Guen, M. Dauvergne, A. Orcesi, and C. Cremona, "Life cycle assessment of cement: Are existing data and models relevant to assess the cement industry's climate change mitigation strategies? A literature review", *Constr. Build. Mater.,* vol. 411, p. 134415, 2024. [http://dx.doi.org/10.1016/j.conbuildmat.2023.134415]

[5] Y. Zheng, X. Xi, H. Liu, C. Du, and H. Lu, "A review: Enhanced performance of recycled cement and CO2 emission reduction effects through thermal activation and nanosilica incorporation", *Constr. Build. Mater.,* vol. 422, p. 135763, 2024. [http://dx.doi.org/10.1016/j.conbuildmat.2024.135763]

[6] S. Danieli, J.S.A. Neto, E.G. Soares, T.F. Oliveira, B.L. Brito, and A.P. Kirchheim, "Shaping a sustainable path: Exploring opportunities and challenges in carbon capture and utilization in cement and concrete industry", *Cement,* vol. 19, p. 100135, 2025. [http://dx.doi.org/10.1016/j.cement.2025.100135]

[7] S. Boudreau, E. Lam, and F.M. Kerton, "Accessing biominerals from by-products wasted by the seafood processing industry", *RSC Sustainability,* vol. 4, no. 1, pp. 28-60, 2026. [http://dx.doi.org/10.1039/D5SU00527B]

[8] D.N. Beatty, and W.V. Srubar, "Nucleation effects of coccoliths in portland cement", *Matter,* vol. 8, no. 7, p. 102100, 2025. [http://dx.doi.org/10.1016/j.matt.2025.102100]

[9] R.K. Majhi, S. Shin, J. Kim, and S.K. Patro, "Towards sustainable cement: Review of blended binder systems and performance-based specification strategies", *Mater. Today Sustain.,* vol. 34, p. 101328, 2026. [http://dx.doi.org/10.1016/j.mtsust.2026.101328]

[10] F. Jin, M. Zhao, M. Xu, and L. Mo, "Maximising the benefits of calcium carbonate in sustainable cements: Opportunities and challenges associated with alkaline waste carbonation", *npj Mater. Sustain.,* vol. 2, p. 1, 2024. [http://dx.doi.org/10.1038/s44296-024-00005-z]

[11] E.A. Chavez Panduro, M. Torsæter, K. Gawel, R. Bjørge, A. Gibaud, A. Bonnin, C.M. Schlepütz, and D.W. Breiby, "Computed X-ray tomography study of carbonate precipitation in large Portland cement pores", *Cryst. Growth Des.,* vol. 19, no. 10, pp. 5850-5857, 2019. [http://dx.doi.org/10.1021/acs.cgd.9b00864]

[12] Z. Xiao, J. Zhang, X. Hu, A. Khaskhoussi, P. He, X. You, X. Su, W. Chen, and C. Shi, "An overview on polymorphs of calcium carbonate formed during carbon mineralization of cementitious materials", *J. Sustain. Cem. Based Mater.,* vol. 14, no. 5, pp. 1005-1027, 2025. [http://dx.doi.org/10.1080/21650373.2025.2471820]

[13] A.L. Silva, E.R. Kohlman Rabbani, and M. Shakouri, "Seashell powder as a sustainable alternative in cement-based materials: A systematic literature review", *Sustainability,* vol. 17, no. 2, p. 592,

2025.
[http://dx.doi.org/10.3390/su17020592]

[14] B.A. Tayeh, M.W. Hasaniyah, A.M. Zeyad, and M.O. Yusuf, "Properties of concrete containing recycled seashells as cement partial replacement: A review", *J. Clean. Prod.,* vol. 237, p. 117723, 2019.
[http://dx.doi.org/10.1016/j.jclepro.2019.117723]

[15] A.M. Zeyad, I.S. Agwa, A.M. Alshoaibi, H.M. Magbool, and N.B. Frahat, "Optimization of HSC using crab shell-based cement substitutes through a response surface methodology study", *Arab. J. Sci. Eng.,* vol. 51, no. 10, pp. 13387-13417, 2026.
[http://dx.doi.org/10.1007/s13369-025-11004-0]

[16] C. Giosuè, R. Jbr, J. Gonzàlez-Camejo, C. Andreola, M.L. Ruello, A.L. Eusebi, F. Fatone, and V. Corinaldesi, "Supplementary cementitious material from food industry: Closing the loop using mollusk seashell waste", *Constr. Build. Mater.,* vol. 492, p. 143013, 2025.
[http://dx.doi.org/10.1016/j.conbuildmat.2025.143013]

[17] H.M. Hamada, A. Al-Attar, M.K. Askar, S. Beddu, A. Majdi, and A.M. Humada, "Recycled seashells as sustainable aggregates in concrete: Advancing waste management and enhancing performance: A comprehensive review", *J. Build. Eng.,* vol. 110, p. 113067, 2025.
[http://dx.doi.org/10.1016/j.jobe.2025.113067]

[18] Z. Li, L. Wang, J. Tang, and J. Seidel, "Nano-mechanical variations in chamber units of dry cuttlebone", *J. Mech. Behav. Biomed. Mater.,* vol. 170, p. 107117, 2025.
[http://dx.doi.org/10.1016/j.jmbbm.2025.107117] [PMID: 40616930]

[19] N. Suwannasingha, A. Kantavong, S. Tunkijjanukij, C. Aenglong, H.B. Liu, and W. Klaypradit, "Effect of calcination temperature on structure and characteristics of calcium oxide powder derived from marine shell waste", *J. Saudi Chem. Soc.,* vol. 26, no. 2, p. 101441, 2022.
[http://dx.doi.org/10.1016/j.jscs.2022.101441]

[20] A. Mao, N. Zhao, Y. Liang, and H. Bai, "Mechanically efficient cellular materials inspired by cuttlebone", *Adv. Mater.,* vol. 33, no. 15, p. 2007348, 2021.
[http://dx.doi.org/10.1002/adma.202007348] [PMID: 33675262]

[21] Y. Ait Hamdan, H. Oudadesse, and K.A. Zerhouni, "Thermal-structural behavior, physicochemical characterization and 3D printing of aragonite (CaCO3) derived from cuttlebone waste", *Research Square,* 2026.
[http://dx.doi.org/10.21203/rs.3.rs-9442407/v1]

[22] S. Mirzabagheri, G. Derhamjani, S. Maharati, Z. Ziaee, F. Vatankhah, and D. Mirzabagheri, "Using cuttlebone powder to produce green concrete", *J. Appl. Eng. Sci.,* vol. 8, no. 2, pp. 25-28, 2018.
[http://dx.doi.org/10.2478/jaes-2018-0014]

[23] H.A. Shah, and W. Meng, "Improving the mechanical properties of cement paste with carbonated blast furnace slag by tailoring CaCO3 polymorphs and increasing carbonation degree", *Cement Concr. Compos.,* vol. 165, p. 106343, 2026.
[http://dx.doi.org/10.1016/j.cemconcomp.2025.106343]

[24] L. Li, M. Cao, and H. Yin, "Comparative roles between aragonite and calcite calcium carbonate whiskers in the hydration and strength of cement paste", *Cement Concr. Compos.,* vol. 104, p. 103350, 2019.
[http://dx.doi.org/10.1016/j.cemconcomp.2019.103350]

[25] ASTM International, *ASTM C150/C150M-19: Standard Specification for Portland Cement,* ASTM International: West Conshohocken, PA, USA, 2019.
[http://dx.doi.org/10.1520/C0150_C0150M-19]

[26] ASTM International, *ASTM C305-20: Standard Practice for Mechanical Mixing of Hydraulic Cement Pastes and Mortars of Plastic Consistency,* ASTM International: West Conshohocken, PA, USA, 2020.
[http://dx.doi.org/10.1520/C0305-20]

[27] ASTM International, *ASTM C109/C109M-20: Standard Test Method for Compressive Strength of Hydraulic Cement Mortars (Using 2-in. or [50-mm] Cube Specimens),* ASTM International: West Conshohocken, PA, USA, 2020.
[http://dx.doi.org/10.1520/C0109_C0109M-20]

[28] ASTM International, *ASTM C511-21: Standard Specification for Mixing Rooms, Moist Cabinets, Moist Rooms, and Water Storage Tanks Used in the Testing of Hydraulic Cements and Concretes,* ASTM International: West Conshohocken, PA, USA, 2021.
[http://dx.doi.org/10.1520/C0511-21]